Research Article

Lixin Qiu, Haiyan Qi*, Wenbo Li, Jun Li, Rokayya Sami, N. I. Aljuraide, Hala M. Abo-dief, Mahmoud Helal

Nitrogen and boron co-doped carbon dots probe for selectively detecting Hg^{2+} in water samples and the detection mechanism

https://doi.org/10.1515/chem-2024-0114
received September 7, 2024; accepted November 6, 2024

Abstract: Mercury ions represent hazardous contaminants with significant adverse effects on human health, wildlife, and vegetation. Therefore, it is crucial to create a sensitive and trustworthy technique for identifying mercury ions. In this study, nitrogen and boron co-doped carbon dots (N,B-CDs) were created via a one-step hydrothermal approach, employing citric acid, polyethyleneimine, and boric as precursors. The resulting N,B-CDs exhibited spherical morphology with an average diameter of 2.60 nm and emitted blue fluorescence with peak emissions at 442 nm (λ_{em}) upon excitation at 360 nm (λ_{ex}), yielding a fluorescence quantum yield of 27.34%. Remarkably, N,B-CDs, without any surface modifications, functioned as a direct "turn-off" probe, enabling swift, highly selective Hg^{2+} detection. The N,B-CDs probe could measure Hg^{2+} in the linear ranges of 0.40–22 μM and 22–208 μM, with a detection limit of 0.12 μM. The detection mechanism was attributed to dynamic quenching interactions between N,B-CDs, and Hg^{2+}. Additionally, the probe was used to detect Hg^{2+} in both tap and river water, and the recovery rates ranged from 87.20 to 108.20% (RSD <4.89%). These findings highlighted the method's considerable practical potential for detecting Hg^{2+} in environmental water.

Keywords: nitrogen and boron co-doped carbon dots, detection of Hg^{2+}, one-step hydrothermal approach, dynamic quenching

1 Introduction

Mercury ions (Hg^{2+}) constitute a significant group of harmful pollutants in modern industrial environments, exerting severe negative effects on human, animal, and plant life [1–4]. Upon accumulation to critical concentrations in water, food, and the environment, they infiltrate biological systems, persisting for extended periods. The affinity of mercury ions for sulfhydryl groups leads to various health issues, including DNA damage, renal and hepatic dysfunction, neural and cerebral impairment, heightened susceptibility to myocardial infarctions, and more [5–7]. The Standards for Drinking Water Quality of China and Environmental quality standards for surface water establish a stringent threshold of 0.001 mg/L for permissible mercury levels in tap and river water. Consequently, the development of a robust and highly sensitive technique for mercury ion detection becomes imperative. Existing methodologies, including atomic absorption spectrometry, atomic emission spectrometry, and inductively coupled plasma-mass spectrometry, suffer from drawbacks such as specialized expertise and expensive equipment requirements. [8] Fluorescence probes have become a viable method for detecting Hg^{2+}. While conventional fluorescence probes incorporate small organic molecules and semiconductor quantum dots,

* **Corresponding author: Haiyan Qi,** College of Chemistry and Chemical Engineering, Qiqihar University, No. 42, Wenhua Street, Qiqihar, 161006, China, e-mail: qhy120@sina.com
Lixin Qiu: College of Chemistry and Chemical Engineering, Qiqihar University, No. 42, Wenhua Street, Qiqihar, 161006, China, e-mail: qlx980124@163.com
Wenbo Li: College of Chemistry and Chemical Engineering, Qiqihar University, No. 42, Wenhua Street, Qiqihar, 161006, China, e-mail: lwb010508@163.com
Jun Li: College of Chemistry and Chemical Engineering, Qiqihar University, No. 42, Wenhua Street, Qiqihar, 161006, China; Technology Innovation Center of Industrial Hemp for State Market, Regulation, Qiqihar, 161006, China, e-mail: 837534403@qq.com
Rokayya Sami: Department of Food Science and Nutrition, College of Sciences, Taif University, P.O. Box 11099, Taif, 21944, Saudi Arabia, e-mail: rokayya.d@tu.edu.sa
N. I. Aljuraide: Department of Physics, Turabah Branch, Turabah University College, Taif University, P.O. Box 11099, Taif, 21944, Saudi Arabia, e-mail: n.aljareed@tu.edu.sa
Hala M. Abo-dief: Department of Science and Technology, University College-Ranyah, Taif University, P.O. Box 11099, Taif, 21944, Saudi Arabia, e-mail: h.abodeif@tu.edu.sa
Mahmoud Helal: Department of Mechanical Engineering, Faculty of Engineering, Taif University, P.O. 11099, Taif, 21944, Saudi Arabia, e-mail: mo.helal@tu.edu.sa

these materials possess intrinsic shortcomings like toxicity and poor water solubility. Carbon dots (CDs), a new type of luminous material, offer several strong points, including low toxicity, admirable water solubility, strong biocompatibility, economical preparation, and enduring stability [9–11]. In recent years, CDs have been widely used in sensor areas [12–14]. Especially in the detection of mercury ions, CDs fluorescent probes have been increasingly reported [15–19]. In practical applications, fluorescence quantum yield and detection time are important indices.

In our study, we prepared nitrogen and boron co-doped carbon dots (N,B-CDs) with high fluorescence quantum yield (27.34%) and quick exam time (40 s) using a one-step hydrothermal synthesis approach (Scheme 1). Our functional CDs demonstrated a specific ability for detecting Hg^{2+}, with a decrease in fluorescence attributed to dynamic quenching. Furthermore, the utility of N,B-CDs extended successful detection of Hg^{2+} in samples.

2 Results and discussion

2.1 Preparation and optimization of N,B-CDs

The schematic representation of the N,B-CDs preparation process and the mechanism for Hg^{2+} detection are outlined in Scheme 1. Notably, the reaction's crucial aspects, including reactant mass ratios, reaction temperature, and duration, were identified as primary drivers of CDs formation. The outcomes of the optimization experiments are presented in Figure 1. It is evident that the synthesis conditions significantly impact the results. Specifically, the best parameters were found to be 200°C and 10 h for the reaction and a reactant mass ratio of 3:1 for polyethyleneimine to boric acid. Utilizing these optimal parameters, the QY of the resulting CDs was measured to be 27.34%. The CDs obtained under these specific parameters were designated as N,B-CDs.

2.2 Characterization of N,B-CDs

HRTEM was used to determine the size distribution and morphology of N,B-CDs. The HRTEM findings revealed a well-dispersed and approximately spherical configuration of N,B-CDs, with an average size of 2.60 nm and particle sizes ranging from 1.58 to 3.69 nm (Figure 2a and b). The average particle size analyzed with DLS was 2.73 nm (inset in Figure 2b). Further structural analysis was conducted using X-ray diffraction (XRD) analysis (Figure 2c), revealing a broad diffraction peak at 20.9°, indicative of the amorphous carbon structure of N,B-CDs.

FTIR spectroscopy was utilized to recognize the existence of functional groups or bonds within the compound. The FTIR spectrum (Figure 2d) exhibited a broad peak spanning 3,720–3,045 cm^{-1}, illustrating N–H and O–H bonds. The peaks at 2,929–2,817 cm^{-1} were attributed to C–H, while the peak at 1,710 cm^{-1} represented the carbonyl group. The peaks at 1,558, 1,348, and 1,151 cm^{-1} were attributed to C=C, C–N, and C–O bonds. The peaks at 1,454, 1,348, and 1,151 cm^{-1} were associated with the bending vibrations of saturated C–H bonds, C–N stretching, and B–O stretching. These FTIR

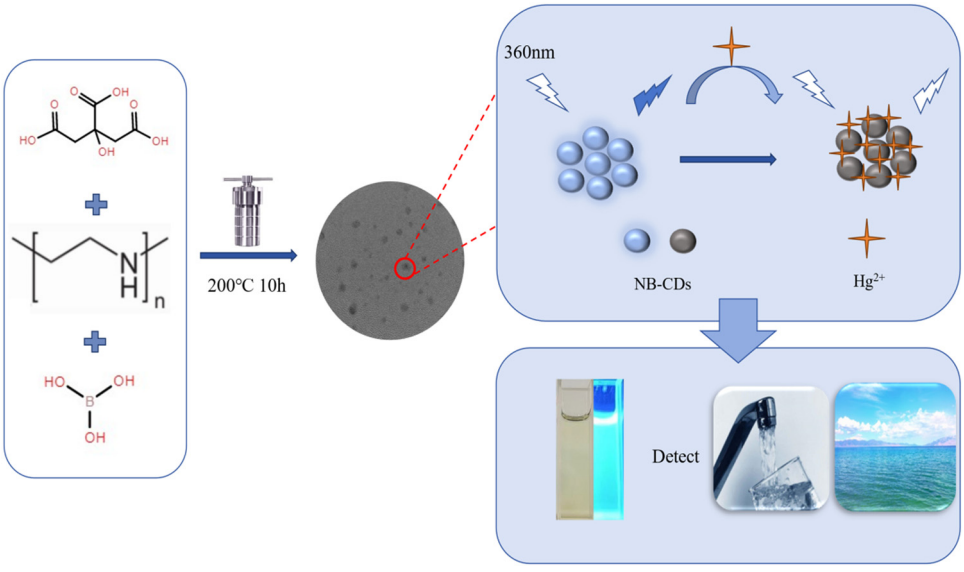

Scheme 1: Schematic synthesis and detection of N,B-CDs.

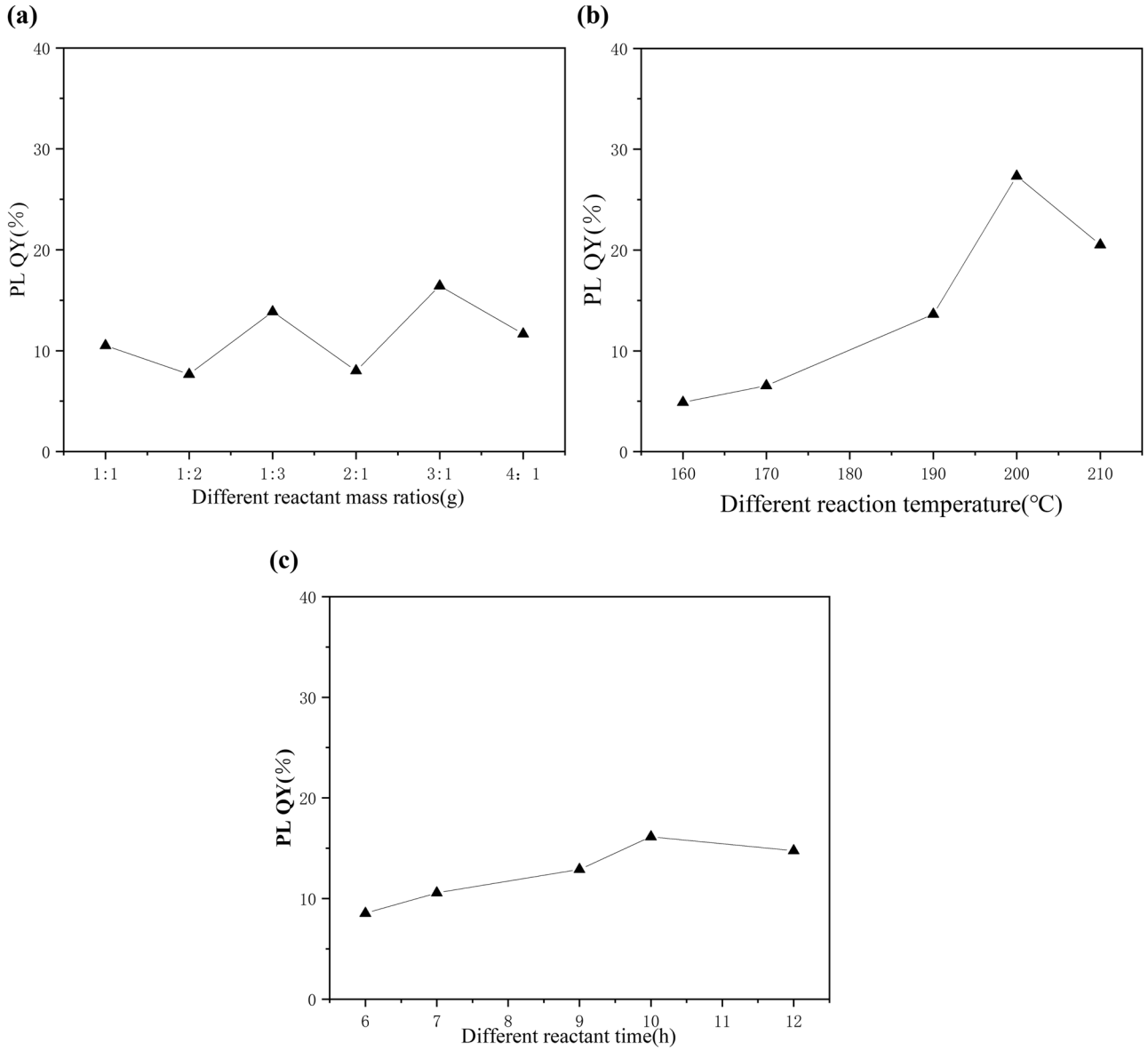

Figure 1: QYs at (a) various reactant mass ratios, (b) different reaction temperatures, and (c) varied reaction times.

findings suggested successful boron (B) doping and the existence of –NH and C═O of N,B-CDs [20–27].

XPS analysis was employed for the detailed characterization of chemical and elemental composition. The XPS survey spectrum (Figure 3a) depicted four peaks at 284.80, 531.12, 399.78, and 191.21 eV, corresponding to C, N, O, and B, respectively. Elemental composition percentages were determined as follows: C (66.7%), O (21.8%), N (10.6%), and B (0.9%) (Figure 3b).

The high-resolution XPS spectra revealed specific chemical environments for each element. The C1s spectrum (Figure 3c) displayed three peaks at 283.939 (C═C), 285.22 (C–N), and 287.09 (C–O/C═O) eV. The N1s spectrum (Figure 3d) exhibited two distinctive peaks at 398.62 eV (N–H) and 400.59 eV (C–N). The O1s spectrum (Figure 3e) depicted three peaks at 531.55 (C–O/C═O), 530.9 6 (B–O), and 530.03 eV (O–H). The B1s spectrum (Figure 3f) featured a single peak at 191.26 eV, attributed to B–O bonds [28–33]. Notably, the XPS and FTIR findings were in agreement, which further supported the presence of amino and carbonyl groups and the effective addition of boron (B) doping.

2.3 Optical characteristics of N,B-CDs

The UV-Vis spectrum of N,B-CDs exhibited two distinctive peaks: one at 243 nm owing to the π–π* transition of carbon nuclei, and another at 358 nm associated with the n–π* transition of C═O and surface defects arising from the nitrogen-

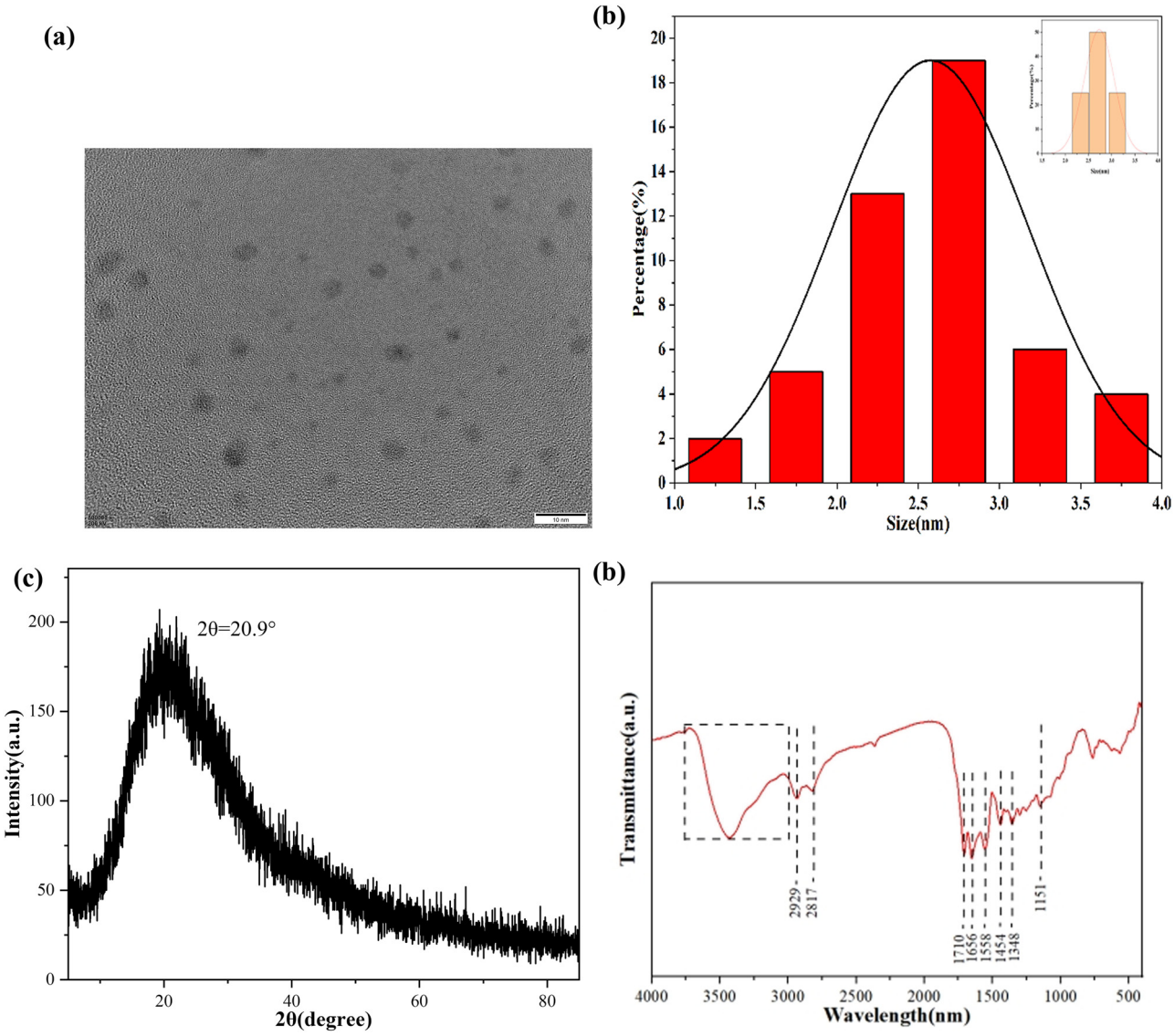

Figure 2: (a) HRTEM image, (b) size distribution, (c) XRD, and (d) FTIR spectra.

containing conjugate structure [34–38]. The appearance of the N,B-CDs aqueous solution was visually depicted in a complementary inset in Figure 4, appearing pale yellow in natural light and emitting luminous blue color when exposed to a 365 nm UV lamp.

The λ_{ex} and λ_{em} of N,B-CDs were observed at 360 and 442 nm (Figure 5a). Furthermore, the Commission Internationale de l'Éclairage (CIE) color coordinates of N,B-CDs (0.1930, 0.1037) highlighted their characteristic blue fluorescence upon UV irradiation (Figure 5b). The fluorescence spectra revealed a gradual decrease in intensity with increasing excitation wavelengths from 300 to 390 nm, accompanied by a minor red-shift of the emission peak from 439 to 446 nm (Figure 5c). This red-shift was more pronounced upon normalization (Figure 5d), indicating a favorable low wavelength dependence of the experimentally produced N,B-CDs.

Various factors, including illumination, ionic strength, and pH, were crucial in assessing the durability of N,B-CDs. The effect of ion concentration on intensity was evaluated by introducing varying contents of NaCl (0.2–1.0 mM). The intensity of N,B-CDs exhibited negligible changes (Figure 6a), illustrating their robust salt tolerance and potential applicability for biological applications.

The photographic stability was assessed by monitoring changes in fluorescence intensity under continuous 365 nm UV light irradiation over 120 min (Figure 6b) and indicated a gradual reduction in intensity, stabilizing at approximately 65 min. The intensity of N,B-CDs diminished to 32.83% after irradiation for 90 min.

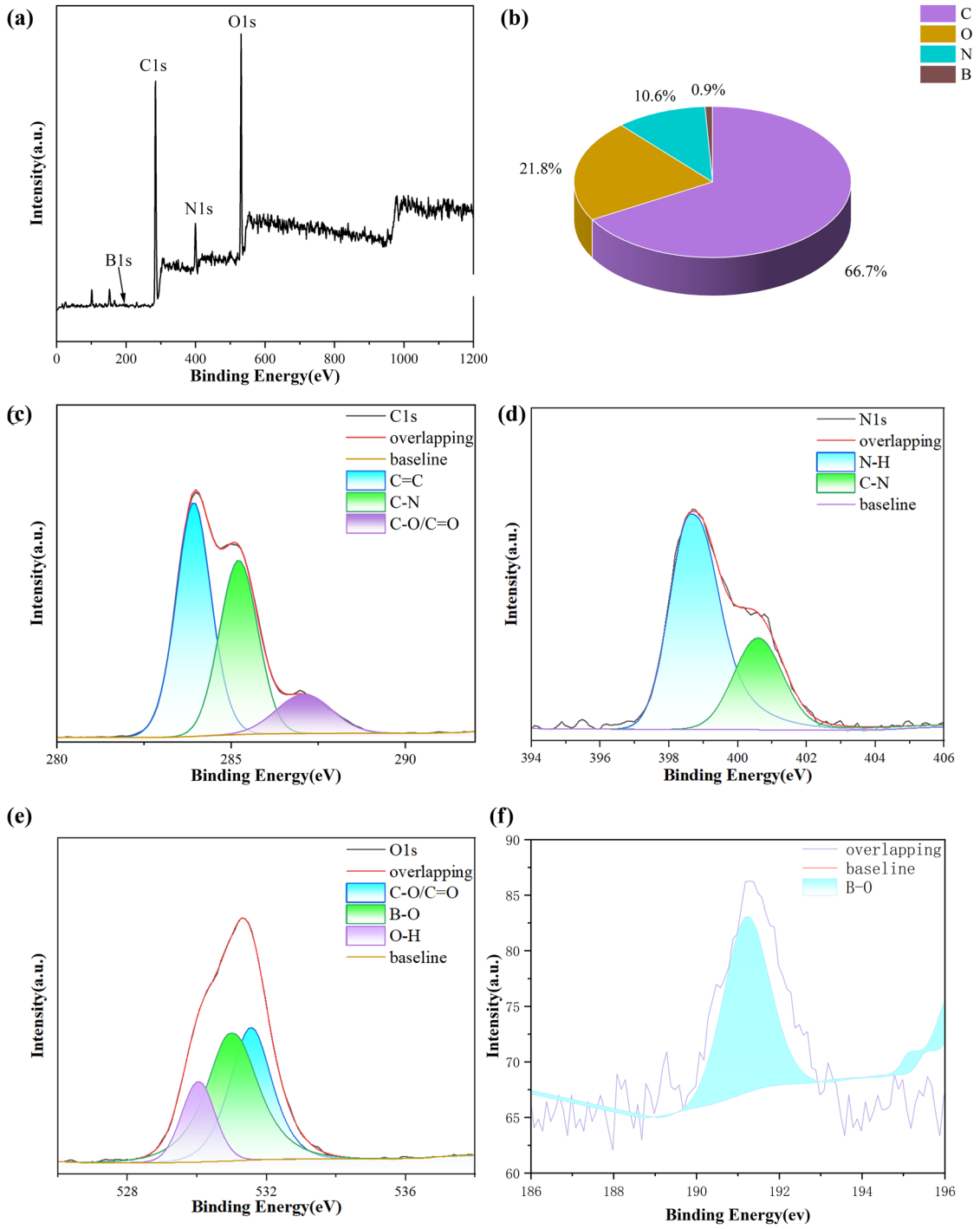

Figure 3: (a) XPS spectrum; (b) element content diagram; and the XPS spectra of (c) C1s, (d) N1s, (e) O1s, and (f) B1s.

The pH effects (Figure 6c) revealed rapid fluorescence intensity enhancement within an acidic range (pH 1–5), followed by a decrease in weakly acidic to strongly basic environments (pH 6–14). This observation underscored the robust fluorescence stability of N,B-CDs across a spectrum from weakly acidic to strongly alkaline conditions. For subsequent experiments, a pH of 5.0 was chosen as the optimal condition.

The practical applicability of N,B-CDs in assays was assessed by evaluating key performance indicators, including response time and interference resistance for Hg^{2+} detection. A crucial aspect for accurate and efficient Hg^{2+} detection is the response time, as both excessively prolonged or short response times can impact experimental precision. As illustrated in Figure 6d, the intensity of N,B-CDs rapidly decreased by 44% within 5 s, followed by a minor

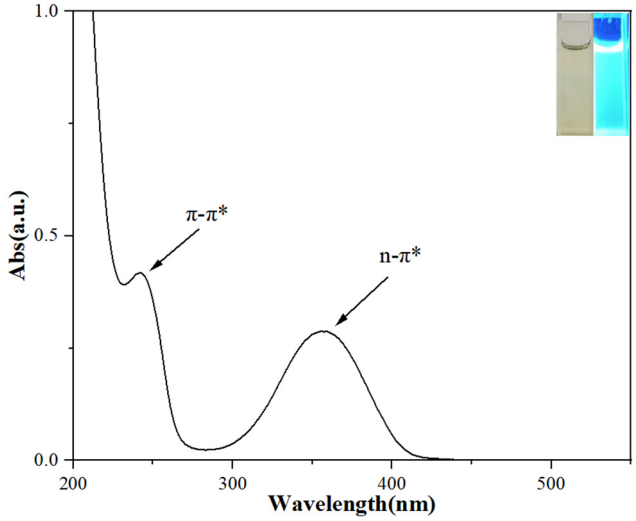

Figure 4: UV-vis spectrum (inset: natural light [left] illumination and UV light [right]).

decrease of 11% within 40 s, and then stabilized until 90 s. To ensure accuracy and credibility, a response time of 40 s was selected for subsequent experiments.

2.4 Hg^{2+} detection

In practical detection, the presence of other substances or metal ions may potentially interfere with the Hg^{2+} detection process. As depicted in Figure 7a, N,B-CDs exhibited a strong response solely to Hg^{2+} while showing negligible response to other substances containing metal ions (Ba^{2+}, Ca^{2+}, Cd^{2+}, K^{+}, Ni^{2+}, Na^{+}, Mg^{2+}, Fe^{3+}, and Cu^{2+}), anions (Cl^{-}, F^{-}, S^{2-}, and NO_3^{-}), organic small molecules (L-Phe, AA, L-Ser, and L-Thr), and antibiotics (amoxicillin, florfenicol, erythromycin, and streptomycin). Furthermore, the addition of interfering substances with Hg^{2+} did not significantly affect fluorescence intensity (Figure 7b). Thus, these

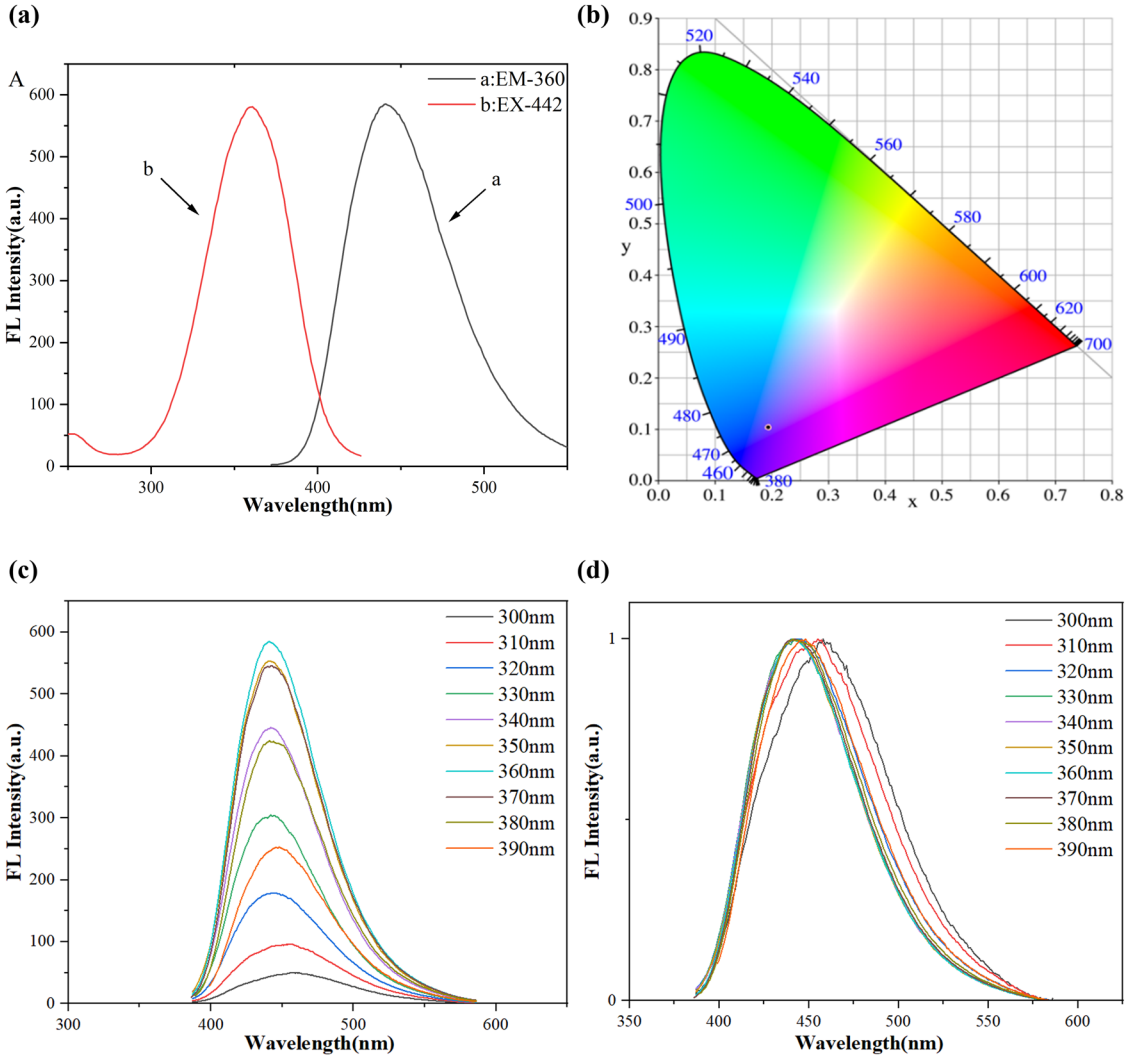

Figure 5: (a) Excitation and emission fluorescence spectra, (b) CIE coordinate diagram, (c) fluorescence spectra (300–390 nm), and (d) normalized fluorescence spectra (300–390 nm).

results conclusively demonstrated the excellent selectivity and resistance to interference of N,B-CDs in Hg^{2+} detection.

To elucidate the capacity of N,B-CDs for Hg^{2+} detection, a range of Hg^{2+} concentrations (0–208 μM) was introduced to N,B-CDs solutions. The intensity at 442 nm gradually decreased with increasing Hg^{2+} concentrations (Figure 8a). The calculated $(F_0 - F)/F_0$ ratio demonstrated a robust linear association with Hg^{2+} concentration within the ranges of 0.40–22 and 22–208 μM (Figure 8b). The resulting equations were $(F_0 - F)/F_0 = (0.01037 \pm 7.06605 \times 10^{-4})$ $[Hg^{2+}] + (0.05929 \pm 0.01226)$ (R^2 = 0.99085), and $(F_0 - F)/F_0 = (0.00156 \pm 3.73145) \times 10^{-4}$ $[Hg^{2+}] + (0.2504 \pm 0.00397)$ (R^2 = 0.99772), respectively, with the limit of detection (LOD, $3\sigma/K$) of 0.12 μM. The N,B-CDs exhibited an extensive detection range and an impressive LOD for Hg^{2+} detection, as summarized in Table 1, outperforming previous studies.

2.5 Quenching mechanism

The UV spectrum of N,B-CDs (Figure 9a) revealed two evident peaks at 243 and 355 nm. Upon introduction of Hg^{2+}, the peak at 243 nm weakened, possibly due to the reduction of the conjugated aromatic π system triggered by Hg^{2+}. However, no new compounds were formed. Further insight into the detection mechanism was gained through examination of fluorescence lifetime. Notably, the addition of Hg^{2+} induced a significant change in the fluorescence lifetime, resulting in a decrease from 11.53 to 7.45 ns (Figure 9b). This decrease unequivocally indicated that the observed fluorescence quenching was attributed to the dynamic quenching process. Additionally, the emission spectrum of N,B-CDs and the UV spectrum of Hg^{2+} did not overlap, elucidating that there was no resonance energy transfer between them (Figure 9c). Based

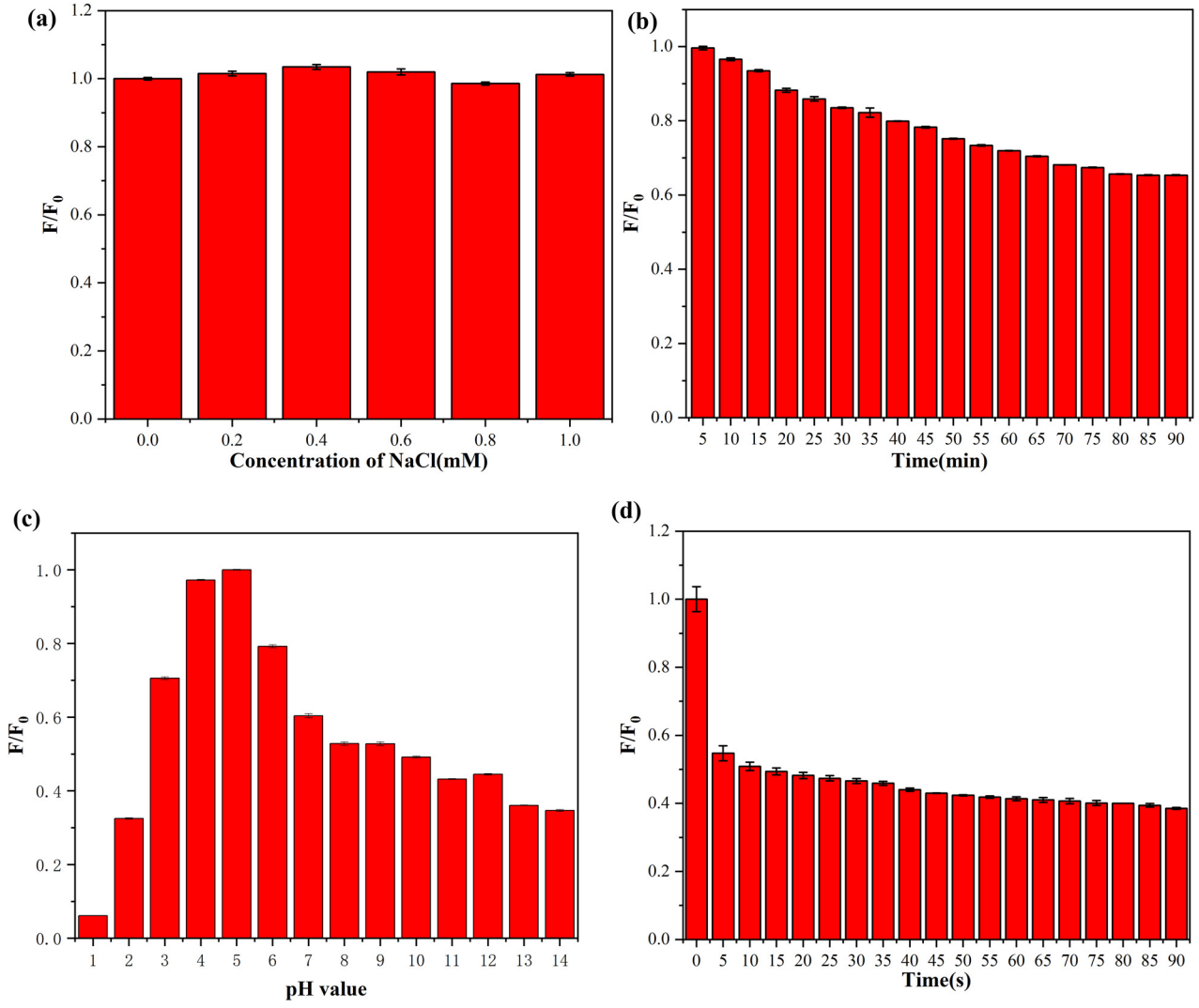

Figure 6: The fluorescence intensity at (a) ion strength, (b) continuous UV irradiation (365 nm), (c) different pH values, and (d) response time of N,B-CDs for Hg^{2+} detection.

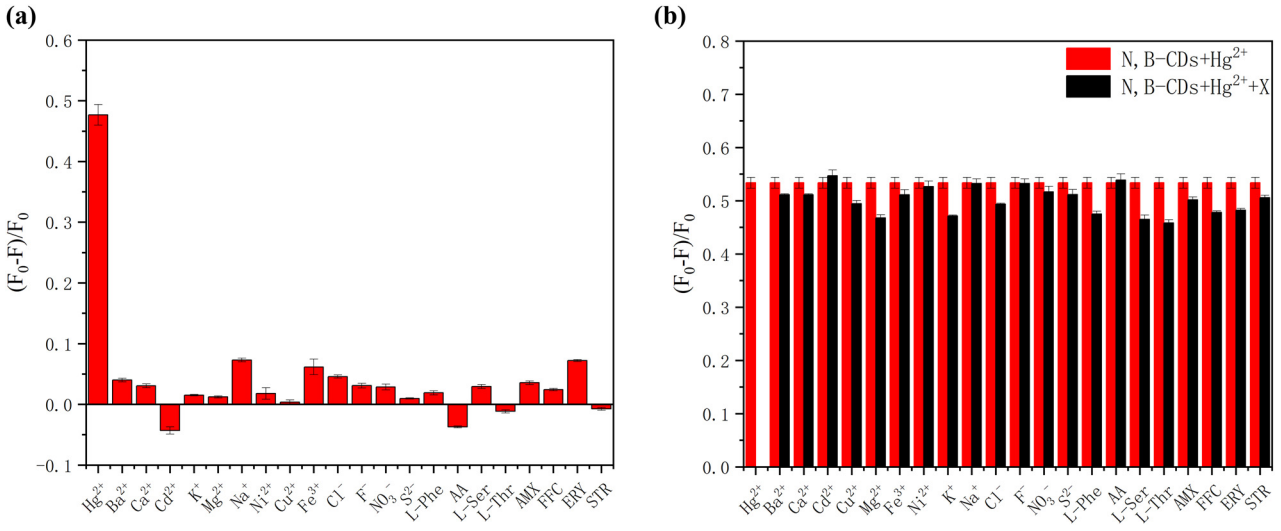

Figure 7: (a) Selective and (b) anti-interference experiments.

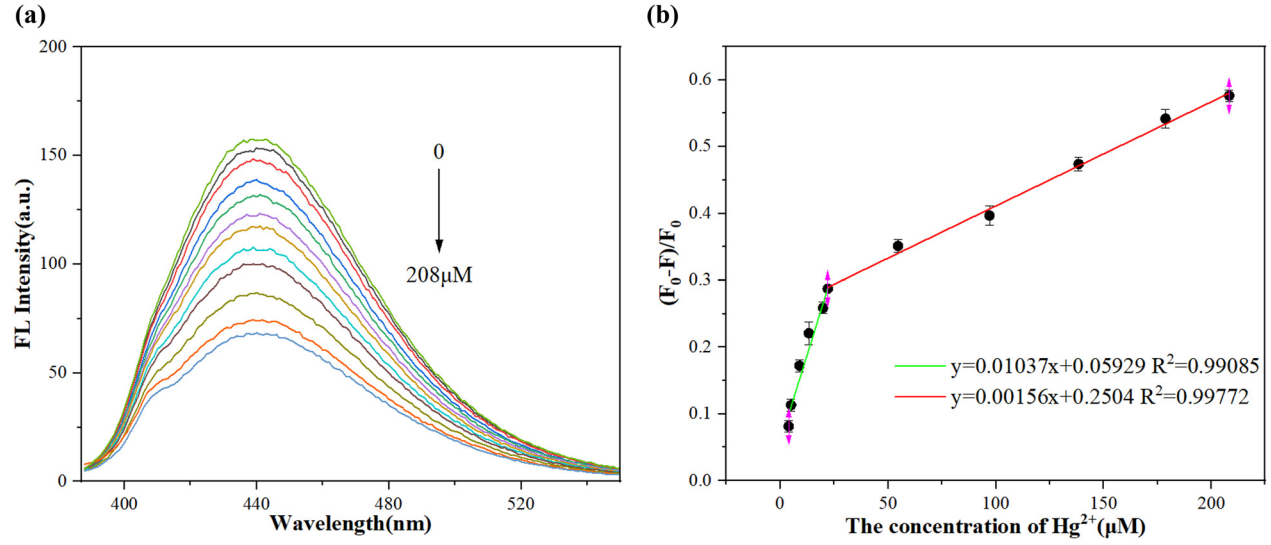

Figure 8: (a) Response of N,B-CDs to Hg^{2+} and (b) the fit curve between $(F_0 - F)/F_0$ and Hg^{2+}.

Table 1: Comparative analysis of Hg^{2+} detection methods

	Linear range (μM)	LOD (μM)	Ref.
N,S-CDs	0.7–15	0.54	Lee et al. [39]
N-CDs	0.9–10	0.15	Zhang et al. [40]
N,S-CDs	0–120	0.16	Liu et al. [41]
CDs-MnO_2	0.16–16	37	Xu et al. [42]
CDs	0.95–50	0.27	Zheng et al. [43]
Y-CDs	20–150	0.12	Liu et al. [44]
N,B-CDs	**0.40–208**	**0.12**	This work

Bold values represent to emphasize our work.

on these results, it was deduced that in the dynamic quenching process, the excited-state electrons of our CDs transferred to the 6s orbits of Hg^{2+}, which caused fluorescence quenching.

2.6 Detection of specimen

The Hg^{2+} level of local tap water and Neijing river water was measured using N,B-CDs in order to clarify practical utility. Table 2 reveals the absence of detectable Hg^{2+} in tap and river water. Additionally, three distinct concentrations

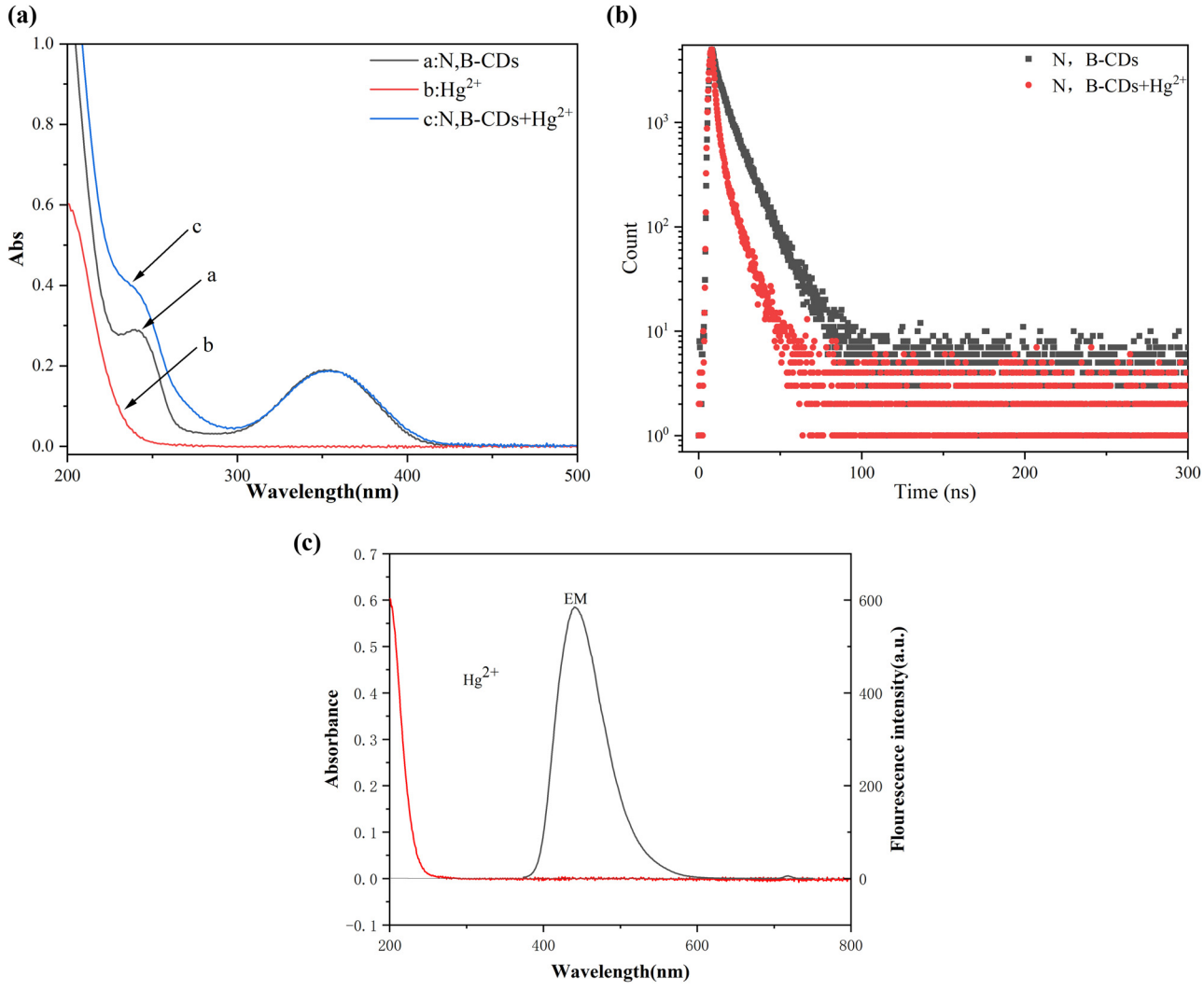

Figure 9: (a) Ultraviolet spectra, (b) fluorescence time spectra, and (c) the UV spectrum of Hg^{2+} and fluorescence spectrum of N,B-CDs.

Table 2: Detection of Hg^{2+} in practical samples

Sample	Added (μM)	Measured (μM)	Recovery (%)	RSD (%)
Tap water	5	4.74	94.48	4.89
	10	9.67	96.70	4.79
	15	15.48	103.20	1.94
River water	5	4.36	87.20	3.67
	10	10.88	108.80	2.79
	15	14.34	95.60	3.57

of Hg^{2+} (5, 10, and 15 μmol/L) were introduced to tap water to assess the performance of N,B-CDs. Remarkably, the recovery rates ranged from 87.20 to 108.20% (RSD <4.89%), underscoring the robust practicality and precision of our N,B-CDs within real sample contexts.

3 Conclusion

In summary, we successfully developed a highly selective fluorescence sensing probe utilizing N,B-CDs for Hg^{2+} detection. Notably, our N,B-CDs, without any surface modifications, demonstrated exceptional efficacy as direct fluorescent probes for Hg^{2+} detection based on dynamic quenching. This innovative approach underscored the potential of the CDs for real-world monitoring of Hg^{2+}, offering a valuable tool for environmental assessment.

Funding information: This research was supported by The Fundamental Research Funds in Heilongjiang Provincial Universities (145309525) and The Special Scientific Research Fund of Powerful Province Through Higher Education (GJQSCYH-2022001). The authors extend their appreciation to Taif University, Saudi Arabia, for

supporting this work through project number (TU-DSPP-2024-79).

Author contributions: Lixin Qiu and Haiyan Qi: conceptualization, writing – original draft preparation; Wenbo Li: data curation; Haiyan Qi, Jun Li and Rokayya Sami: funding acquisition; Rokayya Sami: software and supervision; N. I. Aljuraide, Hala M. Abo-dief, and Mahmoud Helal: writing-review and editing.

Conflict of interest: No conflicts of interest are disclosed by the writers.

Ethical approval: The conducted research is not related to either human or animal use.

Data availability statement: All data generated or analyzed during this study are included in this published article and its supplementary information files.

References

[1] Li GF, Lu MG, Li SQ, Yang M, Zhang YL, Zhang YL, et al. A novel fluorescent "OFF-ON" sensing strategy for Hg (II) in water based on functionalized gold nanoparticles. Chemosphere. 2022;303:135174. doi: 10.1016/j.chemosphere.2022.135174.

[2] Zheng LG, Sun RY, Hintelmann H, Zhu JM, Wang RW, SonkeL JE. Mercury stable isotope compositions in magmatic-affected coal deposits: New insights to mercury sources migration and enrichment. Chem Geol. 2018;479:86–101. doi: 10.1016/j.chemgeo.2017.12.032.

[3] Awalludin AS, Ramachandran P, Lee HL, Jarujamrus P. Hydrothermal synthesis of nitrogen-doped graphene quantum dots as a fluorescent probe to detect mercury (II) ions in an aqueous sample. Emergent Mater. 2022;5(1):133–43. doi: 10.1007/s42247-022-00365-z.

[4] Li YX, Lee JY, Lee H, Hu CC. Highly fluorescent nitrogen-doped carbon dots for selective and sensitive detection of Hg^{2+} and ClO^{-} ions and fluorescent ink. J Photochem Photobiol. 2021;405:112931. doi: 10.1016/j.jphotochem.2020.112931.

[5] Pundi A, Chang C. Recent developments in the preparation, characterization, and applications of chemo sensors for environmental pollutants detection. J Env Chem Eng. 2023;11(5):110346. doi: 10.1016/j.jece.2023.110346.

[6] Lan MH, Zhang JF, Chui YS, Wang H, Yang QD, Zhu XY, et al. A recyclable carbon nanoparticle-based fluorescent probe for highly selective and sensitive detection of mercapto biomolecules. J Mater Chem B. 2015;3:127–34. doi: 10.1039/c4tb01354a.

[7] Zhou WY, Mo FW, Sun ZS, Luo JB, Fan JQ, Zhu HN, et al. Bright red-emitting P, Br co-doped carbon dots as "OFF-ON" fluorescent probe for Cu^{2+} and L-cysteine detection. J Alloy Compd. 2022;897:162731. doi: 10.1016/j.jallcom.2021.162731.

[8] Zhao QL, Zhang ZL, Huang BH, Peng J, Zhang M, Pang DW. Facile preparation of low cytotoxicity fluorescent carbon nanocrystals by electrooxidation of graphite. Chem Commun. 2008;41:5116–8. doi: 10.1039/b812420e.

[9] Yuan L, Jiang L, Liu Z, Xiang YY, Song F, Tu YJ. Selective and sensitive simultaneous detection of tartrazine and Hg^{2+} based on N-doped yellow-greenfluorescent carbon dots. Dye Pigment. 2022;209:110893. doi: 10.1016/j.dyepig.2022.110893.

[10] Lee H, Su YC, Tang HH, Lee YS, Lee JY, Hu CC, et al. One-pot hydrothermal synthesis of carbon dots as fluorescent probes for the determination ofmercuric and hypochlorite ions. Nanomaterials. 2021;11(7):1831. doi: 10.3390/nano11071831.

[11] Lu WB, Qin XY, Liu S, Chang GH, Zhang YW, Luo YL, et al. Economical, green synthesis of fluorescent carbon nanoparticles and their use as probes for sensitive and selective detection of mercury (II) ions. Anal Chem. 2012;84(12):5351–7. doi: 10.1021/ac3007939.

[12] Alhazzani K, Alanazi AZ, Ibrahim H, Mostafa AM, Barker J, Mahmoud AM, et al. L-asparaginase-mediated pH shift and carbon dot fluorescence modulation: A sensitive ratiometric method forquantifying L-asparagine in diverse potato varieties under variable storage conditions. Food Chem. 2025;463:141396. doi: 10.1016/j.foodchem.2024.141396.

[13] AlQarni AO, Mahmoud AM, Ali R, El-Wekil MM. Colorimetric and fluorometric dual-mode determination of hypochlorite based onredox-mediated quenching. RSC Adv. 2023;13(46):32492–501. doi: 10.1039/d3ra05870k.

[14] Mahmoud AM, Alqahtani YS, El-Wekil MM, Ali ABH. Ratiometric sensing of azithromycin and sulfide using dual emissive carbon dots: a turn on-off-on approach. J Fluoresc. 2024;1–13. doi: 10.1007/s10895-024-03737-2.

[15] Thanomsak S, Kerdphon S, Sirikulkajorn A, Tuntulani T, Janrungroatsakul W. A simple fluorescent "on-off-on" nanosensor based on nitrogen-doped carbon dots for selective detection of Hg^{2+} and thiamine. Opt Mater. 2024;151:115336. doi: 10.1016/j.optmat.2024.115336.

[16] Hao YQ, Ji FY, Li TT, Tian MM, Han X, Chai F. Portable smartphone platform utilizing AIE-featured carbon dots for multivariate visual detection for Cu^{2+}, Hg^{2+} and BSA in real samples. Food Chem. 2024;446:138843. doi: 10.1016/j.foodchem.2024.138843.

[17] Zhou YH, Shi JH, Ning J, Hu JZ, Zhou YM. Carbon dots-based modularization fluorescent probe for simultaneous detection of Hg^{2+} and Cu^{2+} in water, cells and zebrafish. Dye Pigment. 2023;214:111232. doi: 10.1016/j.dyepig.2023.111232.

[18] Zhang SB, Yan HD, Li HN, Xu TT, Li H, Wang CK, et al. Carbon dots as specific fluorescent sensors for Hg^{2+} and glutathione imaging. Microchim Acta. 2023;190(6):224. doi: 10.1007/s00604-023-05805-z.

[19] Yuan L, Jiang L, Liu Z, Xiang YY, Song F, Tu YJ. Selective and sensitive simultaneous detection oftartrazine and Hg^{2+} based on N-doped yellow-greenfluorescent carbon dots. Dye Pigment. 2023;209:110893. doi: 10.1016/j.dyepig.2022.110893.

[20] Dong GH, Lang K, Yang HO, Zhang WZ, Bai LM, Chen SJ, et al. Facilesynthesis of N, P-doped carbon dots from maize starch via a solvothermal approach for the highly sensitive detection of Fe^{3+}. Rsc Adv. 2020;10:33483–9. doi: 10.1039/d0ra06209j.

[21] Masoud MS, Ibrahim AA, Khalil EA, El-Marghany A. Spectral propertiesof some metal complex derived from uracil–thiouracil and citrazinic acid compounds. Spectrochim Acta A. 2007;67:662–8. doi: 10.1016/j.saa.2006.07.046.

[22] Sarkar S, Dutta S, Ray C, Dutta B, Chowdhury J, Pal T. A two-component hydrogelator from citrazinic acid and melamine: synthesis, intriguing role of reaction parameters and iodine adsorption study. Crystengcomm. 2015;17:8119–29. doi: 10.1039/c5ce01001b.

[23] Zhang R, Chen W. Nitrogen-doped carbon quantum dots: Facile synthesisand application as a “turn-off” fluorescent probe for detection of Hg^{2+} ions. Biosens Bioelectron. 2014;55:83–90. doi: 10.1016/j.bios.2013.11.074.
[24] Siriwardana K, Nettles CB, Vithanage BCN, Zhou YD, Zou SL. Dongmao Zhang. On-resonance fluorescence, resonance Rayleigh scattering, and Ratio metric resonance synchronous spectroscopy of molecular- and quantum dots- fluorophores. Anal Chem. 2016;88:9199–206. doi: 10.1021/acs.analchem.6b02420.
[25] Liao S, Zhao XY, Zhu FW, Chen M, Wu ZL, Song XZ, et al. N-doped carbon quantum dot-based “off-on” fluorescent sensor for silver ion and cysteine. Talanta. 2018;180:300–8. doi: 10.1016/j.talanta.2017.12.040.
[26] Ding H, Zhang P, Wang TY, Kong JL, Xiong HM. Nitrogen-doped carbon derived from polyvinyl pyrrolidone and their multicolor cell imaging. Nanotechnology. 2014;25:205604. doi: 10.1088/0957-4484/25/20/205604.
[27] Bao RQ, Chen ZY, Zhao ZW, Sun X, Zhang JY, Hou LR, et al. Green and facilesynthesis of nitrogen and phosphorusco-doped carbon quantum dots towards fluorescent ink and sensing applications. Nanomaterials. 2018;8:386. doi: 10.3390/nano8060386.
[28] Babar G, Garje SS. Nitrogen and phosphorus co-doped carbon dots for selective detection of nitro explosives. ACS Omega. 2020;5:2710–7. doi: 10.1021/acsomega.9b03234.
[29] Yang F, He X, Wang CX, Cao Y, Li Y, Yan LN, et al. Controllable and eco-friendly synthesis of P-riched carbon quantum dots and its application for copper (II) ion sensing. Appl Surf Sci. 2018;448:589–98. doi: 10.1016/j.apsusc.2018.03.246.
[30] Xu Q, Pu P, Zhao JJ, Dong CB, Gao C, Chen YS, et al. Preparation of highly photoluminescent sulfur-doped carbon dots for Fe(iii) detection. J Mater Chem A. 2015;3:542–6. doi: 10.1039/c4ta05483k.
[31] Xing Y, Yang M, Chen X. Fabrication of P and N co-doped carbon dots for Fe^{3+} detection in serum and lysosomal tracking in living cells. Biosensors. 2023;13:230. doi: 10.3390/bios13020230.
[32] Zhao D, Zhang ZX, Liu XM, Zhang R, Xiao XC. Rapid and low-temperature synthesis of N, P co-doped yellow emitting carbon dots and their applications as antibacterial agent and detection probe to Sudan Red I. Mat Sci Eng C-Mater. 2021;119:111468. doi: 10.1016/j.msec.2020.111468.
[33] Shi J, Ni G, Tu JC, Jin XY, Peng J. Green synthesis of fluorescent-carbon dots for sensitive detection of Fe^{2+} and hydrogen peroxide. J Nanopart Res. 2017;19:1–10. doi: 10.1007/s11051-017-3888-5.
[34] Sarkar S, Chowdhury J, Dutta S, Pal T. A pH dependent Raman and surface enhanced Raman spectroscopic studies of citrazinic acid aided bytheoreticalcalculations. Spectrochim Acta A. 2016;169:108–5. doi: 10.1016/j.saa.2016.06.023.
[35] Reckmeier CJ, Schneider J, Xiong Y, Häusler J, Kasák P, Schnick W, et al. Aggregated molecular fluorophores in the ammono thermal synthesis of carbon dot. Chem Mater. 2017;29:10352–61. doi: 10.1021/acs.chemmater.7b03344.
[36] Gao F, Ma SY, Li J, Dai K, Xiao XC, Zhao D, et al. Rational design of high quality citric acid-derived carbon dots by selecting efficient chemical structure motifs. Carbon. 2017;112:131–41. doi: 10.1016/j.carbon.2016.10.089.
[37] Wang L, Zhou H. Green synthesis of luminescent nitrogen-doped carbon dots from milk and its imaging application. Anal Chem. 2014;86:8902–5. doi: 10.1021/ac502646x.
[38] Su YT, Zhang M, Zhou NL, Shao MN, Chi C, Yuan P, et al. Preparationof fluorescent N, P-doped carbon dots derived from adenosine 5’-monophosphate for use in multicolor bioimaging of adenocarcinomic human alveolar basalepithelial cells. Microchim Acta. 2017;184:699–706. doi: 10.1007/s00604-016-2039-5.
[39] Lee H, Su YC, Tang HH, Lee YS, Lee JY, Hu CC, et al. One-pot hydrothermal synthesis of carbon dots as fluorescent probes for the determination ofmercuric and hypochloriteions. Nanomaterials. 2021;11:1831. doi: 10.3390/nano11071831.
[40] Zhang C, Wu S, Yu Y, Chen F. Determination of thiourea based on the reversion of fluorescence quenching of nitrogen doped carbon dots by Hg^{2+}. Spectrochim Acta A. 2020;227:117666. doi: 10.1016/j.saa.2019.117666.
[41] Liu H, Xu H, Li H. Detection of Fe^{3+} and Hg^{2+} ions by using high-fluorescent carbon dots doped with S and N as fluorescence probes. J Fluoresc. 2022;32:1089–98. doi: 10.1007/s10895-022-02921-6.
[42] Xu Y, Chen X, Chai R, Xing CF, Li HR, Yin XB. A magnetic/fluorometric bimodal sensor based on a carbon dots MnO_2^- platform for glutathione detection. Nanoscale. 2016;8:13414–21. doi: 10.1039/c6nr03129c.
[43] Zheng YB, Wan YD, Wei Y, Yu YC. One-pot synthesis of dual-emissivecarbon dots for ratiometric fluorescent determination of Hg^{2+}. J Fluoresc. 2023;33(5):1941–8. doi: 10.1007/s10895-023-03154-x.
[44] Liu HD, Li HW, Du KZ, Xu HX. Yellow fluorescent carbon dots sensitivedetection of Hg^{2+} and its detection mechanism. Mater Today Commun. 2022;33:104880. doi: 10.1016/j.mtcomm.2022.104880.